Diffraction-limited performance of flat-substrate reflective imaging gratings patterned by DUV photolithography

Christoph M. Greiner, D. Iazikov, and T. W. Mossberg

LightSmyth Technologies, 860 W Park St, Ste 250, Eugene ,OR 97401
cgreiner@lightsmyth.com

Abstract: We report on the first demonstration of flat substrate imaging gratings fabricated by deep ultraviolet (DUV) photoreduction lithography, which uniquely offers sub-100-nm resolution and spatial coherence over centimeter scales. Reflective focusing gratings, designed according to holographic principle, were fabricated on 300-mm silicon wafers by immersion DUV lithography. Spatial coherence of the fabrication process is evident in measured diffraction-limited imaging function. Flat-substrate gratings, with lines of arbitrary spacing and curvature, offer both dispersion and general spatial wavefront transformation combining the function of multiple optical elements. Fabrication at the sub-100-nm resolution level allows high-line-count, low-order efficient gratings even into the deep ultraviolet region. Nanoreplication of gratings at the wafer level provides a pathway to devices of ultimate low cost.

©2006 Optical Society of America

OCIS codes: (050.1950) Diffraction Gratings; (050.1976) Diffractive Optics; (090.1760) Computer Holography; (090.2890) Holographic Optical Element; (110.3960) Microlithography

References and links

1. C. Greiner, D. Iazikov, and T. W. Mossberg, "Lithographically-fabricated planar holographic Bragg reflectors," J. Lightwave Technol. **22**, 136-145 (2004).
2. J. J. Wang et al., "Wafer-based nanostructure manufacturing for integrated nanooptic devices," J. Lightwave Technol. **32**, 474-485 (2005).
3. W. Bogaerts, V. Wiaux, D. Taillaert, S. Beck, B. Luyssaert, P. Bienstmann, R. Baets, "Fabrication of photonic crystals in Silicon-on-Insulator using 248-nm deep UV photolithography," J. Sel. Top. Quantum. Electron. **8**, 928-934 (2002).
4. M. Settle, M. Salib, A. Michaeli, T. F. Krauss, "Low loss silicon on insulator photonic crystal waveguides made by 193nm optical lithography", Opt. Express **14**, 2440-2445 (2006).
5. S. Ura, Y. Honzawa, T. Suhara, and H. Nishihara, "Reflection-type multiorder grating lens for three ultraviolet wavelengths," Appl. Opt. **38**, 3008-3011 (1999).
6. Y. Hori, F. Sogawa, H. Asakure, M. Kato, and H. Serizawa, " Fabrication of a focusing grating mirror by electron beam lithography," Appl. Opt. **29**, 2522 (1990).
7. S. Ura, T. Sasaki, and H. Nishihara, " Combination of grating lenses for color splitting and imaging," Appl. Opt. **40**, 5819-5825 (2001)
8. S. Ura et al., " Planar reflection grating lens for compact spectroscopic imaging system," Appl. Opt. **42**, 175-180 (2003).
9. G. Fortin, and N. McCarthy, " Chirped holographic grating used as the dispersive element in an optical spectrometer," Appl. Opt. **44**, 4874-4883 (2005).

1. Introduction

For the last forty years, manufacturing technology for diffraction gratings has not changed significantly. Mechanical ruling and interferometric (holographic) exposure of photoresist followed by etch have been the two predominant approaches used to fabricate grating masters from which copies are derived subsequently via replication. Both approaches

#76418 - $15.00 USD Received 25 October 2006; revised 20 November 2006; accepted 21 November 2006
(C) 2006 OSA

provide limited freedom in terms of the complexity of grating lines (spacings and curvatures) that can be written. Since general line spacings and curvatures are required to implement general wavefront transformations, existing fabrication approaches constrain the production of gratings offering beam shaping as well as simple dispersion. As is demonstrated here, deep ultraviolet (DUV) photolithographic patterning tools, supporting nanometer-scale resolution and arbitrary line spacing and curvature, represent a new approach to grating fabrication – one that renders practical a wide range of advanced grating functions wherein both spectral and spatial signal control is provided on a flat substrate.

DUV reduction photolithography provides nanopatterning capability with feature sizes below 100 nm and control of feature placement on the scale of nanometers (yielding high spatial coherence) throughout a field spanning nearly ten square centimeters [1]. For grating and general diffractive optics, today's typical DUV production optical stepper allows one to address and design more than 10^{11} pixels on an individual basis, enabling truly arbitrary patterning at the subwavelength-level. The ability to tailor grating lines arbitrarily allows incorporation of spatial wavefront control based on the principles of thin holograms. Examples of such wavefront control include signal focusing and collimating without the need for curved substrates. At the same time, CMOS and related processes support wafer throughputs exceeding one hundred per hour, making possible volume production of master gratings at low cost. Even lower cost can be achieved by nanoreplicating gratings or general diffractives at the wafer level [2]. Fabrication of diffractives via DUV photolithography, including integrated optics, is presently an evolving research area in the photonics community [1,3,4].

In the present paper, for the first time, we demonstrate the use of DUV photoreduction lithography to fabricate flat-substrate gratings operative to angularly disperse light by color while focusing it in one or two dimensions. The gratings were analytically designed based on holographic principle and point-wise written to a reticle. Final gratings are produced by projecting the reticle with a DUV photolithographic scanner onto silicon wafers. Fabricated devices were tested and found to provide diffraction-limited imaging performance.

Focusing and other grating lenses, fabricated by electron beam lithography, have been demonstrated previously [5-8]. The available spatially coherent field of an e-beam tool is significantly smaller than that of a typical DUV optical stepper/scanner and fabrication of gratings typically requires stitching of multiple fields which can adversely affect spatial coherence. Diffraction-limited performance of e-beam written gratings has been demonstrated for an area of 1 mm^2 [6], but larger gratings [7] have operated beyond the diffraction limit. From a production standpoint, e-beam writing tends to be slow making it unsuitable for high volume production of grating masters.

2. Design

The gratings on which we report were designed for first-order Littrow configuration. Figure 1 illustrates the design process schematically. For two-dimensionally focusing gratings, lines are chosen to coincide with analytically determined interference fringes between two spherical waves: one emerging from point S_0 and one converging toward it. The counter-propagating spherical waves interfere to form concentric shells whose intersection with the grating plane comprises circles having a common center at point C (Fig. 1). The radius of the m^{th} circular grating line is found to be

$$R_m = \left({d_{in}}^2 + 2\left({d_{in}}^2 + a^2\right)^{1/2}\left(\frac{m\lambda}{2}\right) + \left(\frac{m\lambda}{2}\right)^2 \right)^{1/2}. \quad (1)$$

#76418 - $15.00 USD Received 25 October 2006; revised 20 November 2006; accepted 21 November 2006
(C) 2006 OSA

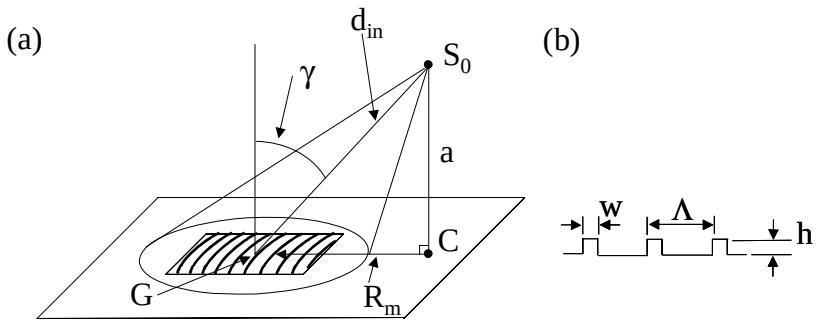


Fig. 1. (a) Schematic illustrating grating design by computer-based holography: d_{in}, source-substrate distance, γ, design input angle, R_m, radius of the m^{th} circular grating line concentric about point C. (b) grating profile: w, linewidth, Λ, grating period, h, line height.

For the tested gratings, $\lambda = 632.8$ nm, $d_{in} = 500$ mm, and $\gamma = 41.4°$ with respect to the substrate normal (see Fig. 1). The relatively large input distance was chosen for testing convenience. Note that for the two-dimensionally focusing gratings, the lines are both variably spaced and curved. For one-dimensionally focusing gratings, which were also fabricated, the lines are chosen as straight and normal to segment CG with the same distances from point C as given in Eq. 1. The line density varies from 2083 to 2105 lines/mm, where the lower value is closest to point C. Note that the design outlined above yields a grating with focal length $f = d_{in}/2 = 25$ cm along segment GS_0 at the design wavelength. The grating lines comprise ~125-nm-wide mesas that, at grating center, are spaced by $\Lambda = 475$ - 480 nm (see Fig. 1(b)). The ~25% duty cycle was motivated by the ray model of corner retroreflection which at Littrow provides blazing function. This model is primarily valid only for larger grating features and future work we be required to evaluate corner blazing relative efficiency. It should be noted that more complex focusing and wavefront transformations can be incorporated into the grating structure by modeling its line pattern after the interference pattern of desired input and output beams evaluated at the grating surface plane. Since DUV photolithographic patterning is essentially pixel based, an arbitrary pattern can be faithfully rendered.

3. Fabrication

Gratings fabricated for one-dimensional and two-dimensional focusing have dimensions of 5×2 mm^2 and 5×4 mm^2, respectively. In all gratings, the longer sides of the patterned region are parallel to segment CG (Fig. 1). The gratings were etched into standard 12-inch-diameter, 750-micron-thick silicon wafers. Curved grating lines were approximated by straight segments controlled in length so that trajectories of segments and curves coincided to better than $\lambda/50$. Data files representing the mirror surface contained the endpoints of the segments. The 5-mm long gratings contained about 10,000 lines and each curved line was represented by typically 9 straight segments. As line curvature increases, segment count for constant fidelity increases. Patterns were written (at four times scale) to a chromium-on-quartz mask using a laser writer. A 193-nm water-immersion DUV optical scanner was employed to image the reticle patterns with 4×-reduction onto 300-mm silicon wafers. The 4× scale reduction allows laser written patterns to reach the 100-nm and lower scale. After resist development the silicon trenches were etched via reactive ion etching. Figure 2(a) shows a fabricated 300-mm silicon wafer containing several hundred diffraction gratings. Figure 2(b) shows cross-sectional scanning electron micrograph pictures of the profile of the one-dimensional focusing grating.

#76418 - $15.00 USD Received 25 October 2006; revised 20 November 2006; accepted 21 November 2006
(C) 2006 OSA

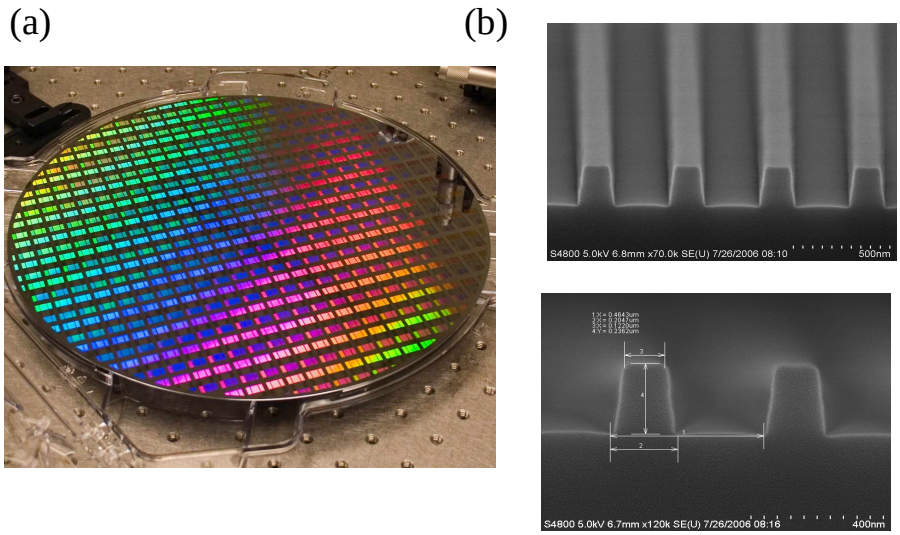


Fig. 2. (a) Photograph of fabricated 12-inch silicon wafer containing focusing diffraction gratings. (b) scanning electron micrographs showing typical partial cross-section of one-dimensional focusing grating, Λ = 464 nm, top line width = 122 nm, bottom line width = 205 nm, h = 236 nm.

4. Results

The optical setup used for evaluation of the fabricated gratings is shown in Fig. 3. According to holographic principle, the grating should reflect the light from a suitably located point source (S_o in Fig. 1) back onto itself. For small displacements of the source from S_o, the location of the focused output signal can be predicted as if it were imaged from a concave mirror at the grating location. This fact was used in implementing the set-up of Fig. 3 so that the output signal beam was displaced from the corresponding input beam. The input beam (λ = 632.8 nm) was focused to a diffraction-limited spot located d_{in} = 50 cm away from the test grating from which input light diverged and substantially overfilled the grating under test (ensuring the input wavefront was approximately spherical). The test gratings were oriented such that the grating lines (at grating midpoint) run perpendicular to the plane (plane of Fig. 3) containing the input and grating normal vector. The input beam

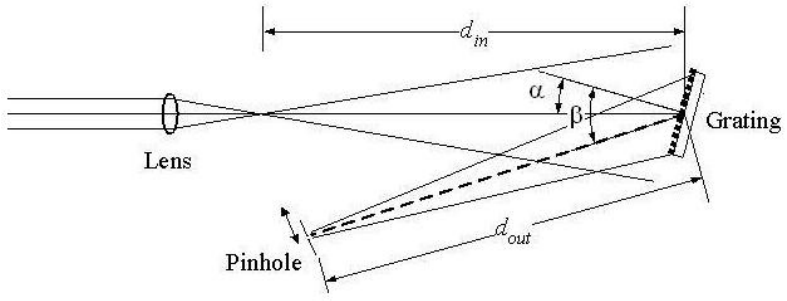


Fig. 3. Schematic of optical test setup. d_{in}, distance of input focal spot to grating, d_{out}, distance of pinhole to grating (image distance). α (β) angle of input (diffracted) beam to grating normal.

#76418 - $15.00 USD Received 25 October 2006; revised 20 November 2006; accepted 21 November 2006
(C) 2006 OSA

was made incident on the grating at an input angle $\alpha = 40°$, close to the Littrow design angle γ, yet causing the diffracted beam to be spatially separated sufficiently to allow characterization by a pinhole (10 μm diameter) positioned at the design output location d_{out}= 50 cm away from the grating and at an angle $\beta = 43.5°$ with respect to it's normal. To test the basic device performance of interest here uncoated silicon gratings with an etched groove depth of h = 140 nm were used. The diffraction efficiency of the 2D focusing gratings was approximately 50 percent (normalized for reflectivity of the uncoated silicon

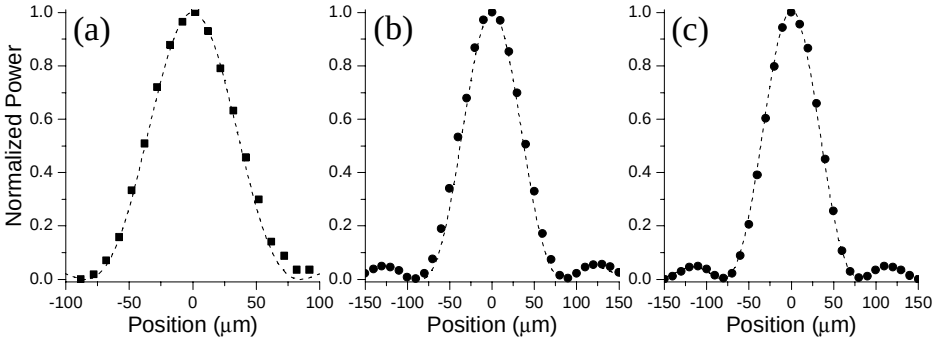


Fig. 4. Power profiles of focused grating output beams. (a) scan along dispersion plane of 1D focusing grating. (b) and (c) scans parallel and normal to dispersion plane, respectively, for 2D focusing grating. Dashed lines, power profiles simulated via Fresnel-Huygens diffraction theory. Observed grating performance is diffraction-limited.

wafer at the same incidence angle) and identical for both s and p–polarization. Work remains to determine optimal efficiency achievable as a function of etch depth, groove duty cycle, and coating.

Figure 4(a) shows as solid squares and dashed line, respectively, the measured and simulated spatial power profile (at focus) produced by a one-dimensional focusing grating as measured in the plane of Fig. 3 with p-polarized input light (perpendicular to the grating lines). Simulated values are produced by diffractive calculation. The one-dimensional focusing grating (variably spaced straight lines) does not focus in the direction normal to Fig. 3. Figure 4(b) and 4(c) show, as solid circles and dashed lines, respectively, the measured and simulated spatial power profile (at focus) produced by the two-dimensionally focusing grating. Figure 4(b) and 4(c) correspond to measurement directions along and perpendicular to the plane of Fig. 3, respectively. Note that the spot size in Fig. 4(b) is slightly wider than in Fig. 4(c) as is expected based on the smaller apparent grating size in the former case. The grating resolution, derived from the measured spot size and the calculated spatial dispersion, exceeds 10^4, i.e. $\Delta\lambda \approx 0.06$ nm at 632.8 nm. Observed grating performance is diffraction limited.

Figure 5(a) shows white light from a pinhole (right) diffracted from three vertically displaced gratings (front of left mount) onto a screen (gratings are shown in Fig. 5(b)). The top and bottom gratings perform 1D focusing along the dispersion direction.

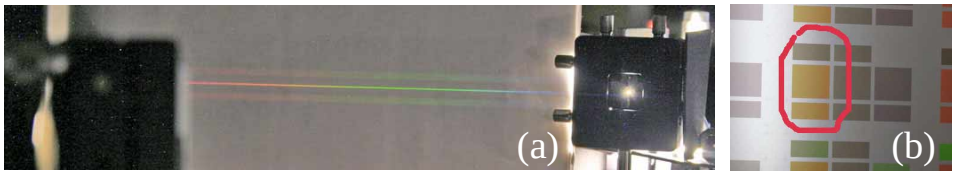


Fig. 5. (a) Photograph of optical test setup showing angularly dispersed grating output of 1D (top and bottom) and 2D (center) focusing gratings. (b) Close-up photograph of gratings on face of grating mount.

#76418 - $15.00 USD Received 25 October 2006; revised 20 November 2006; accepted 21 November 2006
(C) 2006 OSA

Monochromatic input would appear as a thin vertical stripe in the top and bottom rows and white light appears as a continuous unfocused band. The central grating is a 2D focusing grating and it produces the thin color-dispersed horizontal line in the middle of the screen.

The focusing properties of a diffractive optical element can vary as a function of input direction or wavelength. We examine this topic in Fig. 6 for the 1D variable-line-spacing focusing grating by showing the measured (squares) and simulated (line) focusing distance d_{out} as a function of input angle α (Fig. 6(a)) and input wavelength (Fig. 6(b)). The optical setup was identical to that used for Fig. 4(a). For Fig. 6(a), a HeNe laser with $\lambda = 632.8$ nm was used and the input angle α was changed. For Fig. 6b, a tunable ring dye laser was used with $\alpha \approx 38°$. P-polarized (S-polarized) input was used for Fig. 6(a) (Fig. 6(b)). The theoretical curve was obtained via ray tracing incorporating the spatial variation in grating line density.

Agreement between data and theoretically expected behavior is excellent, attesting to the high fidelity provided by the lithographic fabrication process. In Fig. 6(a) d_{out} is seen to vary most strongly for small input angles. We note that it is primarily focusing mediated by variable line spacing that depends on input properties. Focusing derived from line curvature behaves more like a standard curved mirror.

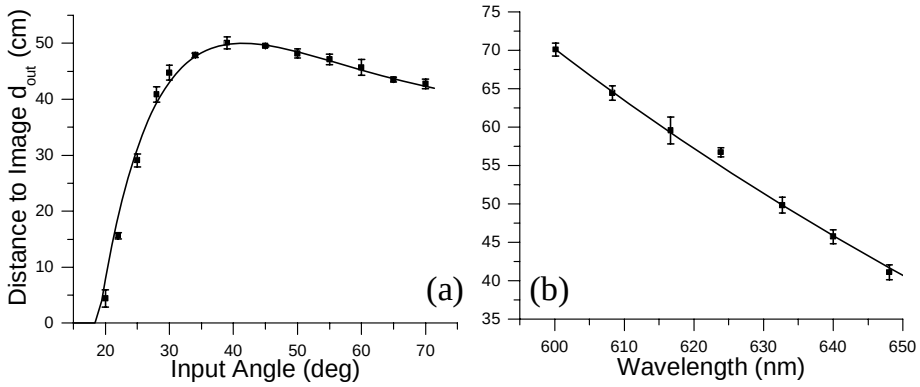


Fig. 6. Image distance d_{out} as a function of input angle for fixed wavelength $\lambda = 632.8$ nm (a) and as a function of input wavelength for fixed input angle $\alpha \approx 38°$ (b). $d_{in} = 50$ cm for both plots.

5. Conclusions

In conclusion, we have demonstrated, for the first time, the use of deep ultraviolet photo-reduction lithography for fabrication of flat-substrate focusing diffraction gratings. Observed focusing performance for design input is diffraction-limited attesting to the extraordinary high fidelity of the lithographic fabrication process. The ability to combine regular dispersive grating function with spatial beam transformations, such as focusing and collimation, via the principles of computer-generated holography and photolithographic fabrication promises to simplify spectrometer systems [9]. Photolithographic tools also provide for the fabrication of multistripe gratings with each grating having a separate pitch and line orientation for broad-band high resolution spectroscopy as needed for example in laser-induced breakdown spectroscopy. Large spatially coherent gratings may be feasible through stitching together multiple DUV fields.

The authors would like to thank the NASA Goddard Space Flight Center and Dr. David Content for support under contract number NNG-06-LA-10C. The authors furthermore thank Professor Hailin Wang and Young-Shin Park of the Oregon Center for Optics for kindly facilitating the dye laser measurements described.

#76418 - $15.00 USD Received 25 October 2006; revised 20 November 2006; accepted 21 November 2006
(C) 2006 OSA